ASME 2012 5th Annual Dynamic Systems and Control Conference joint with the JSME 2012 11th Motion and Vibration Conference
DSCC2012-MOVIC2012
October 17-19, 2012, Fort Lauderdale, Florida, USA

DSCC2012-MOVIC2012-8870

LUMPED-PARAMETER MODELING FOR MENISCUS DYNAMIC ANALYSIS IN IMMERSION FLOW FIELD

Ying Chen[1], Kok-Meng Lee[2,3*], Chun-Yeon Lin[2] and Xin Fu[1]
yingchen@zju.edu.cn; kokmeng.lee@me.gatech.edu*; cylin219@gatech.edu; xfu@zju.edu.cn

[1] State Key Laboratory of Fluid Power Transmission and Control
Zhejiang University
Hangzhou, 310027, China

[2] George W. Woodruff School of Mechanical Engineering
Georgia Institute of Technology
Atlanta, GA 30332-0405

[3] State Key Laboratory of Digital Manufacturing Equipment and Technology
School of Mechanical Engineering
Huazhong University of Science and Technology
Wuhan 430074, China

ABSTRACT

Motivated by the interest to increase production throughputs of immersion lithography machines, wafers are scanned at increasingly high velocities and accelerations, which may result in liquid loss at the receding contact line. The dynamic characteristics of the immersion fluid with free boundary play an important role for fluid management system, and are concerned in various potential immersion unit designs. To offer intuitive insights into the dynamic effects of the immersion fluid due to scan speeds, a lumped-parameter model is developed to characterize the hydrodynamics of the immersion flow process. To validate the model, meniscus behavior information under dynamic conditions is extracted experimentally and analyzed using image processing techniques. The reduced model agrees qualitatively well with the experimental data revealing that parts of the surface tension have an effect on the dynamic response of the menisci similar to that due to a pure time delay in the system.

INTRODUCTION

Immersion lithography has overcome various challenges and become the key production technology (for 45nm node and below) semiconductor devices. As illustrated in Fig. 1(a), the intention of immersion lithography is to increase the index of refraction in the space between the lens and wafer by introducing a high refractive index liquid in place of the low refractive index air that fills the gap in dry lithography. The liquid is provided by an immersion liquid control system as shown in Fig. 1(b), which keeps the liquid fresh and clean, preventing deposition of contaminations [1]. Figures 1(c) shows a prototype of local fill setup applied in an immersion lithography machine [2]. The design of the immersion unit is critical for immersion scanner performance [3].

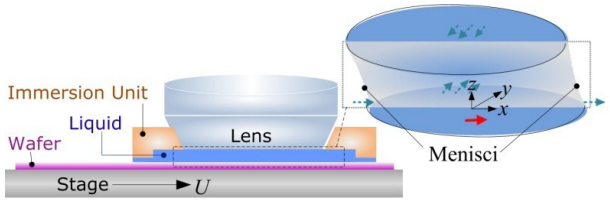

a) Schematic illustrating immersion lithography

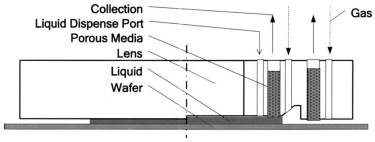

b) Typical immersion unit structure shematics

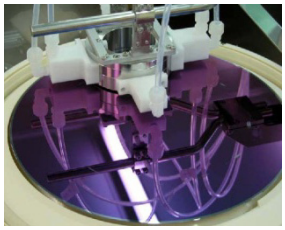

c) Local fill setup (Nikon & TEL collaboration)

FIGURE 1. ILLUSTRATION OF IMMERSION LITHOGRAPHY

In a typical immersion scanner, the liquid is confined by its surface tension within the gap between the projection lens and wafer as the wafer moves at speed *U* as illustrated in Fig. 1(a). The relative motion results in a drag force acting on the liquid by the moving wafer and thus a change in liquid free surfaces.

The wafer traverses through the underlens region in the scanwise direction during exposure. The scan velocity accelerates from zero to a steady velocity U that is maintained for a certain time, and then decelerates until a scan velocity in the opposite direction begins. After finishing a scan, the exposure steps to the next field and this scanning process continues until all of the chips on a wafer are exposed [4]. The interest to increase production throughput has led to higher and higher wafer scan speeds in semiconductor industry. However, the increase in scan speeds potentially results in liquid loss that occurs at the receding contact meniscus (and hence defects on printed patterns).

There has been substantial prior work relative to water leakage like film pulling and meniscus overflow. Most of the published research studies, which focused on the development of the dynamic contact angles of the immersion liquid, have been based primarily on experimental methods to explore the behavior of the advancing and receding menisci. These experimentally obtained dynamic contact angles on different resist-covered surfaces and critical velocities for liquid deposition were observed from a side view using a high-speed camera [5][6]. A semi-empirical model for predicting the critical velocity was based on the 2-D analysis of the receding meniscus [7][8]. To improve the accuracy of the empirical models for different resist-coated surfaces, a 3-D shape of the receding meniscus was created using two camera views (side and below) for analyzing with a lubrication model [9]. Tomographic PIV has also been taken to investigate the internal flow of the confined liquid on a moving substrate, and the flow pattern and liquid shape (at Reynolds number 200) were presented in [10]. While experimental observations provide a means to analyze the shape of receding meniscus relative to the wafer speed, those are relatively costly and limited for design analysis, which is critical for new immersion unit designs and optimization of the fluid management system. There is a need for a rational model offering an in-depth understanding of the 3-D fluid dynamic behaviors, which is essential for developing control strategies against liquid loss under increasingly high scan speed.

The remainder of this paper offers the followings:

1) This paper offers a method for formulating a lumped-parameter model for analyzing the immersion fluid dynamics, and for predicting the liquid transient respond to the wafer motion.
2) Along with an image-based experimental study, a reduced-order dynamic model is presented and validated against actual liquid transient response.
3) Results of the lumped-parameter model and experimental analysis offer an effective means to identify key parameters that significantly affect the liquid meniscus stability.

DYNAMIC MODEL FORMULATION

Figure 2 schematically illustrates the symbols used in modeling and analyzing the dynamics and meniscus stability of the confined liquid under the influence of the scan velocity U, where the liquid (density ρ, surface tension γ, and viscosity μ) is dispensed into a gap (height h). The upper surface of the confined liquid is the bottom of the lens and the immersion unit; for simplicity, only the lens (with diameter d) is depicted in Fig. 2(a). The following assumptions are made in modeling the liquid dynamics:

1) The system is symmetric about the x-z plane.
2) The fluid flow is Newtonian and incompressible.
3) The fluid is dragged entirely by viscous shear; there is no pressure-driven flow such as might be associated with a fluid pump system.
4) There is no relative motion (thus no frictional force) between the projection lens and the liquid.

Kinematics

In Fig. 2, the origin of the reference xyz coordinate system is assigned directly under the lens center on the wafer surface, where x is directed in the scan motion; and z is along the axis of the lens. Figure 2(a) shows the sectional view (an x-z plane through the lens center), where the displacements are measured from their corresponding steady-state values; and the subscripts "+" and "–" denote the receding and advancing meniscus respectively. During scanning, the advancing and receding menisci (with the arc-length $s_{\pm}$), which are characterized by the angles θ_A and θ_R respectively with subscripts "U" and "L" denoting the upper and lower surfaces in Fig. 2(b), change dynamically from their static values.

As the wafer drags the confined liquid along the x direction, the liquid inertia and viscous effects result in different x_- and x_+ displacements and cause some of the confined liquid to displace into $\pm y$ direction. Figure 2(c) illustrates two plan views of the confined liquid where the circular plane contacts the lens while the elliptical plane is on the wafer. Thus, the liquid mass can be conceptually divided into three portions; m_- , m_+ and m_c, where the subscript "c" denotes the quantities in the $\pm y$ direction. The liquid is confined and thus satisfies

$$m_- + m_+ + m_c = \rho \int_0^h \int_{A_{xy}} dA dz \tag{1}$$

Hydrodynamic Force Components

The external forces acting on the confined liquid include the surface tension forces and the viscous frictional force.

Surface Tension Force

Surface tension γ, which acts only at the interfaces of the gas/liquid/solid, is governed by Eq. (2) where [**T**] is the stress tensor; [**E**] is the deviatoric stress tensor; and **n** and **t** are unit normal and unit tangent to the liquid free surface.

$$\mathbf{n}\bullet[\mathbf{T}]\bullet\mathbf{n} = \gamma(\nabla\bullet\mathbf{n}) \quad \text{and} \quad \mathbf{n}\bullet[\mathbf{T}]\bullet\mathbf{t} = (\nabla\gamma)\bullet\mathbf{t} \tag{2a,b}$$

$$\text{where} \quad [\mathbf{T}] = -p[\mathbf{I}] + 2\mu[\mathbf{E}] \text{ and } \mathbf{E} = [\nabla\mathbf{u} + (\nabla\mathbf{u})^{\mathrm{T}}]/2 \tag{3}$$

Equation (2a) expresses the normal component of the stress must balance the curvature force associated with the surface tension on a free surface. Similarly, the tangential stress component on the free surface must be balanced by the local gradient of the surface tension given in Eq. (2b). Since there is no heat exchange or chemical concentration at the interface, surface tension is constant here; in other words, the γ gradient is zero and hence the right side of Eq. (2b) vanishes. The x and y components of the curvature force can be obtained by integrating over the free surface [11]:

$$f_{cx} = \gamma \iint_S (\nabla \bullet \mathbf{n})\mathbf{n} \bullet \hat{\mathbf{x}} dS \quad \text{and} \quad f_{cy} = \gamma \iint_S (\nabla \bullet \mathbf{n})(\mathbf{n} \bullet y) dS \qquad (4a,b)$$

Since the meniscus surface S depends on the displacement, the surface tension is nonlinear.

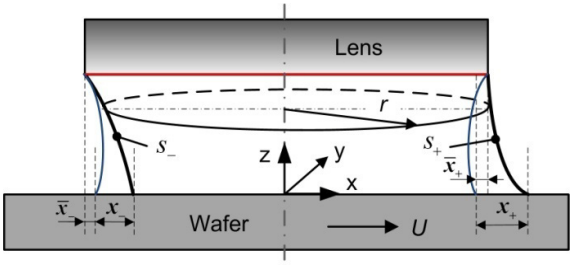

a) Confined liquid deformation from equilibrium

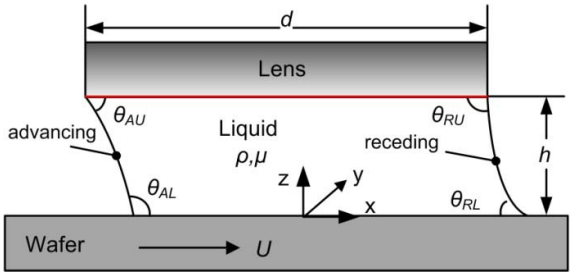

b) Dynamic contact angles between liquid/wafer and liquid/lens

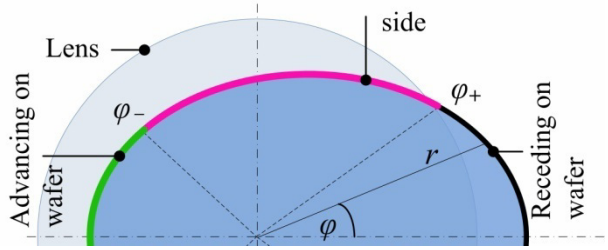

c) Schematics illustrating surface tension approximation

FIGURE 2. LIQUID DEFORMATION AND SYMBOLS

Viscous Frictional Force

In this model, the flow is not pressure driven, there is no pressure gradient along the x-direction; the flow in the gap is approximately as a Couette flow with a linear velocity profile [12], $u=Uz/h$ with the viscous force between the substrate and the liquid, which can be estimated as

$$f = \tau A = \left(\mu \frac{\pi R^2}{h} \right) U \qquad (5)$$

Lumped-Parameter Perturbation Model

Linearized about the steady-state operating point, the effect of wafer scanning on the liquid can be modeled approximately in Fig. 3 as a velocity input U through a damper. As shown in Eq. (4), the effects of surface tension are modeled as massless mechanical springs. Similarly, viscous effects are modeled as dampers. Each of the three masses associates with a massless spring k and a viscous damper as illustrated in Fig. 3. The symbols used to characterize the physical parameters are summarized in Table 1.

Using Newton's second law and the continuity of flow, the following constitutive equations can be obtained from Fig. 3:

$$m_\pm \ddot{x}_\pm = -k_\pm x_\pm + b(\dot{x} - \dot{x}_\pm) \pm pa \qquad (6)$$

$$m_c \ddot{x}_c = pa - k_c x_c - b_c \dot{x}_c \qquad (7)$$

$$\dot{x}_c = (\dot{x}_- - \dot{x}_+) a / a_c \qquad (8)$$

The transfer function, Eq. (9) which relates the displacements of the advancing and receding menisci, can be derived by eliminating pa and x_c from Eq. (7) and Eq. (8) by substituting them into (6), then rearranging the resulting equation, and finally taking Laplace transform with zero initial conditions:

$$\frac{X_\pm(s)}{U(s)} = \frac{\beta_{2\pm} s^2 + \beta_1 s + \beta_{0\pm}}{\alpha_4 s^4 + \alpha_3 s^3 + \alpha_2 s^2 + \alpha_1 s + \alpha_0} \qquad (9)$$

where $\alpha_4 = m_+ m_- + a_r m_c (m_+ + m_-)$;

$\alpha_3 = m_+ b_- + m_- b_+ + a_r m_c (b_+ + b_-) + a_r b_c (m_+ + m_-)$;

$\alpha_2 = m_+ k_- + m_- k_+ + a_r m_c (k_+ + k_-) + a_r k_c (m_+ + m_-) + a_r b_c (b_+ + b_-) + b_+ b_-$;

$\alpha_1 = b_+ k_- + b_- k_+ + a_r b_c (k_- + k_+) + a_r k_c (b_+ + b_-)$;

$\alpha_0 = k_+ k_- + a_r k_c (k_+ + k_-)$;

$\beta_{2\pm} = m_c (b_- + b_+) a_r + m_\mp b_\pm$;

$\beta_1 = b_c (b_- + b_+) a_r + b_+ b_-$;

and $\beta_{0\pm} = k_c (b_- + b_+) a_r + k_\mp b_\pm$.

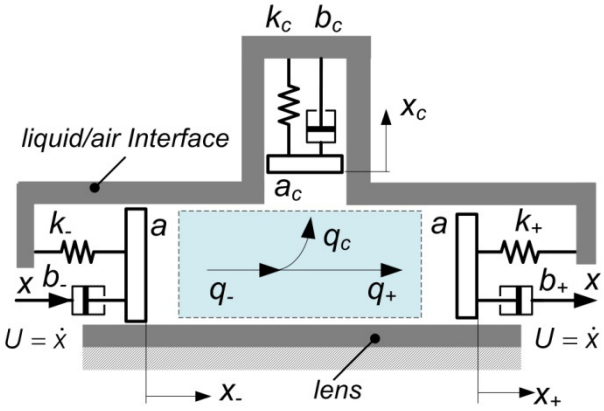

FIGURE 3. LUMPED-PARAMETER MENISCUS MODEL

TABLE 1. PHYSICAL QUANTITY FOR THE MODEL

Parameters	Symbol	Unit
spring constant	$k_{\pm}$, k_c	N/m
viscous friction constant	$b_{\pm}$, b_c	N/(m s)
meniscus displacement	$x_{\pm}$	m
cross-sectional area of meniscus	a, a_c	m^2
volumetric flow rate	$q_{\pm}$, q_c	m^3/s
substrate velocity input	U	m/s

EXPERIMENTAL ANALYSIS

The objectives of the experimental analysis are to validate the lumped-parameter model, and to identify key parameters that significantly affect the liquid meniscus stability. In order to reduce the order of the lumped-parameter model so that a tractable experimental model can be obtained from the transient response, simplifications are made to identify the dominant complex poles and zeros.

Simplified Massless Model ($m_- = m_+ = m_c \ll 1$)

As the thickness of the immersion fluid is no more than 1mm, the fluid inertia is assumed to be negligible compared to the effects of the surface tension and the viscous friction. Eq. (9) reduces to Eq. (10):

$$\frac{X_{\pm}(s)}{U(s)} = K_{\pm}\frac{\omega_n^2\left(T_{\pm}s+1\right)}{s^2+2\varsigma\omega_n s+\omega_n^2} \tag{10}$$

where $\omega_n^2 = \dfrac{k_+k_- + a_r k_c\left(k_+ + k_-\right)}{b_+b_- + a_r b_c\left(b_+ + b_-\right)}$;

$$2\varsigma\omega_n = \frac{b_+k_- + b_-k_+ + a_r k_c\left(b_+ + b_-\right) + a_r b_c\left(k_+ + k_-\right)}{b_+b_- + a_r b_c\left(b_+ + b_-\right)};$$

$$K_{\pm} = \frac{k_{\mp}b_{\pm} + a_r k_c\left(b_+ + b_-\right)}{k_-k_+ + a_r k_c\left(k_- + k_+\right)};$$

and $T_{\pm} = \left(\dfrac{b_c}{k_c}\right)\left[\dfrac{b_+b_- + a_r k_c\left(b_+ + b_-\right)}{b_{\pm}k_{\mp} + a_r k_c\left(b_+ + b_-\right)}\right]$.

Experimental Setup

The experiment setup consists of a quartz lens with a 2mm-diameter injection hole in its center, through which purified water (Elix advantage 5, Millipore) is injected into the gap using a syringe pump (KD Scientific, Model 200 series). The optical glass with magnesium fluoride coating is selected as the substrate, whose wettability is similar to that of typical resist coated wafers. The liquid property and experimental parameters are listed in Table 2. The lens is mounted on a mirror bracket that can be fine-positioned to ensure that the lens and substrate (placed on a translational stage) are parallel. The gap h can be adjusted via a precision micrometer and translation stage. Experimentally, the scan velocity accelerates from zero to a steady velocity U that is maintained for a sufficiently long period to allow for the response to reach a steady state, and then decelerates to rest. Figure 4 shows a typical set of velocity and displacement profiles of the x-stage obtained experimentally.

TABLE 2. PARAMETERS USED IN MODEL/EXPERIMENTS

Parameters	Symbol	Unit	Value
Liquid density (water)	ρ	kg/m^3	998.2
Liquid viscosity	μ	kg/m s	0.001 003
Surface tension	γ	N/m	0.0728
Gap height	h	mm	1.0
Lens diameter	d	mm	8.0
Wafer scan speed	U	mm/s	variable

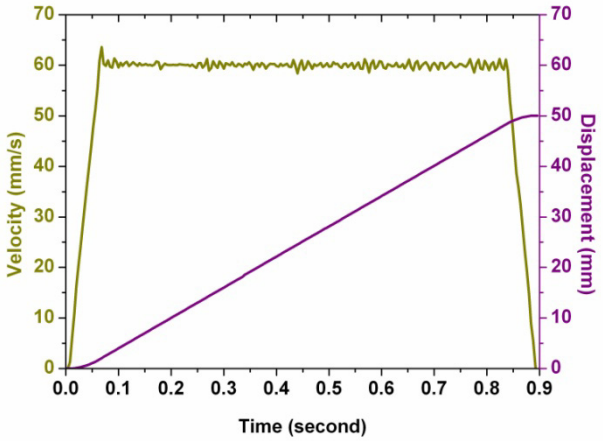

FIGURE 4. X-STAGE VELOCITY AND DISPLACEMENT

The experimental method that was developed to study the dynamic behavior of the meniscus can be found in [13]. During scanning, the free boundary of the confined liquid is recorded using a high-speed camera (FASTCAM-ultima APX) with a micro lens. A fiber optic cold-light source provided an auxiliary back-lighting for the flow field. In each trial, both the upper surface and substrate were cleansed with ethanol and then with purified water using dust-free paper before each scanning. Liquid was then injected incrementally until fully filled the gap between the lens and the substrate. The translational stage was set into motion as soon as the camera was triggered to begin recording. The stage velocity was increased in each trial until liquid loss occurs.

Data Extraction

The motion was recorded at 250 fps and the resolution of images is 17μm/pixel. Hundreds of images were obtained for each trial which provides relatively complete information of the fluid, based on which the meniscus and fluid characteristics can be analyzed using image processing algorithms to obtain the edge data and dynamic contact angles from each frame. For the edge-finding, the flow-field images were converted to grayscale images as shown in Fig. 5(a). Due to non-uniform backlight effects, two different thresholds were used to derive two binary images for the edge extraction; 50/255 for advancing meniscus in Fig. 5(b) and 200/255 for receding meniscus in Fig. 5(c). To

well extract the edges, the connected-component labeling method [14] was used to filter the plots with minor areas so as to obtain the complete image segmentation. Subsequently, the advancing and receding meniscus edges can be obtained as shown in Fig. 5(d).

For the angle detection, the edges of advancing and receding menisci are divided into upper and lower parts for ease of curve fitting [15]. Points on the four sections are subsequently fit to cubic curves in a least squares sense (Fig. 6). Based on the derivatives of these curves, four contact angles can be derived from the inverse tangents of the slopes at the contact points among the fluid, the lens and the substrate.

FIGURE 5. EDGE FINDING PROCESS

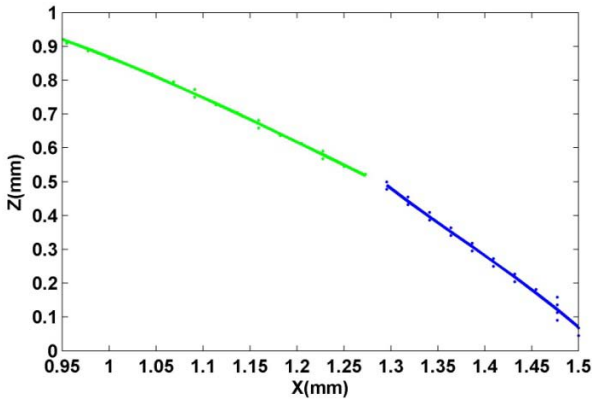

a) Advancing meniscus edge curve fitting

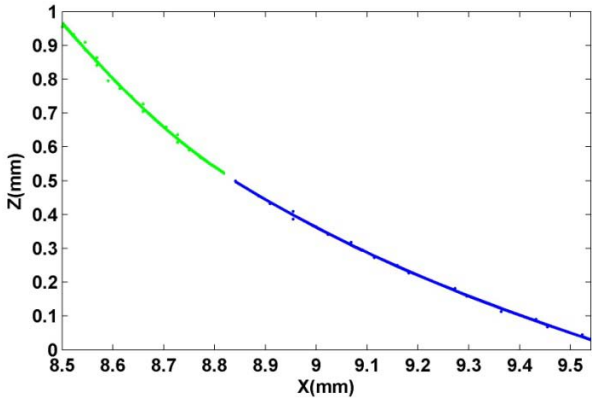

b) Receding meniscus edge curve fitting

FIGURE 6. EDGE DATA AND ASSOCIATED CURVE FITTINGS

Results and Discussion

Results are presented in Figures 7 to 11, and Tables 3 and 4. Figure 7 compares the steady-state advancing and receding menisci at three different scan speeds, 20, 40 and 60 mm/s against that scanned at 65 mm/s where liquid loss occurs without reaching steady state. Figure 8 depicts the four developing dynamic contact angles on the lens surface and substrate surface for two scan speeds, 60 and 65 mm/s.

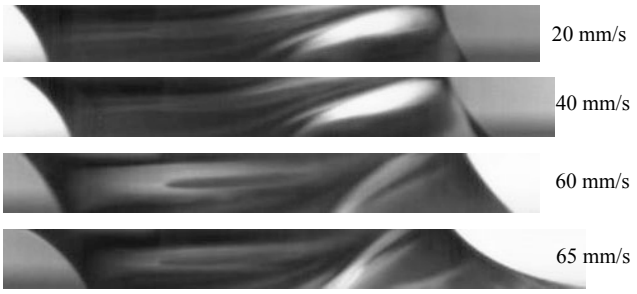

FIGURE 7. EFFECT OF SCAN SPEED ON MENISCI

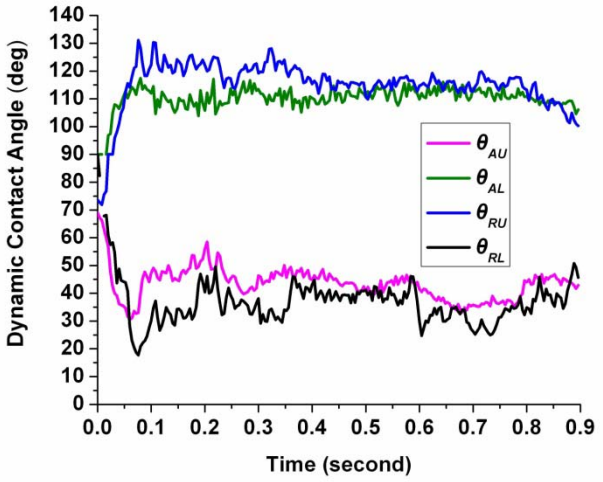

a) Dynamic contact angles with scan speed 60mm/s

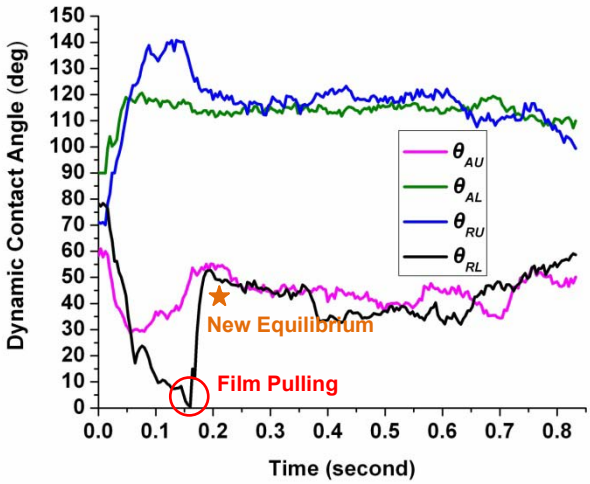

b) Dynamic contact angles with scan speed 65mm/s

FIGURE 8. DYNAMIC CONTACT ANGLES DURING SCANNING

Figures 9 and 10 show typical experimentally obtained transient responses to the velocity input (Fig. 4) for 60 and

65mm/s scan speeds respectively, where the displacements are normalized to their initial steady state values. The experimental data provides a basis for validating the reduced 2nd order model. The comparisons are given in Figs. 9 and 10. For a scan speed of 65mm/s, the transient response of the 2nd order model for the receding meniscus is not plotted where liquid loss occurred as shown in Fig. 11. The 2nd order model for the advancing meniscus derived from experimental data is given in Table 4.

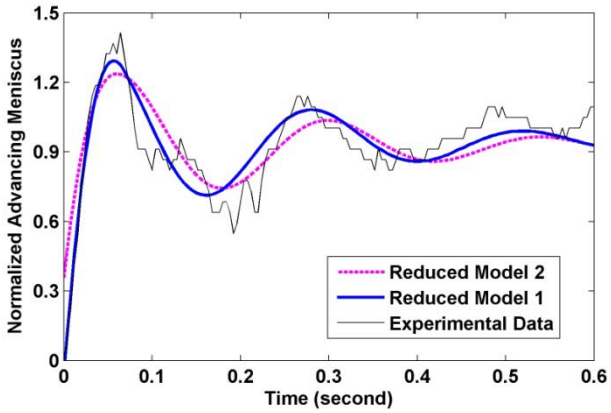

(a) Normalized displacement of the advancing meniscus

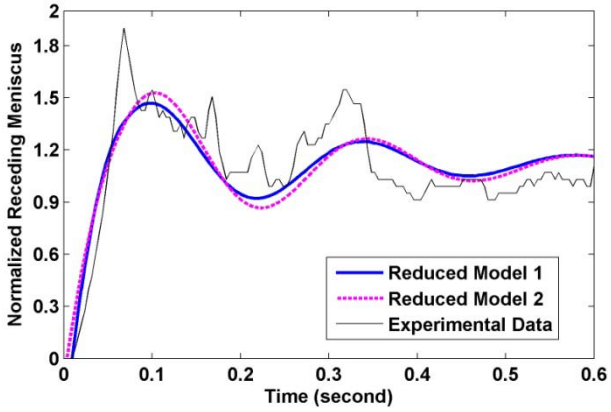

(b) Normalized displacement of the receding meniscus

FIGURE 9. MENISCUS TRANSIENT RESPONSES (60mm/s)

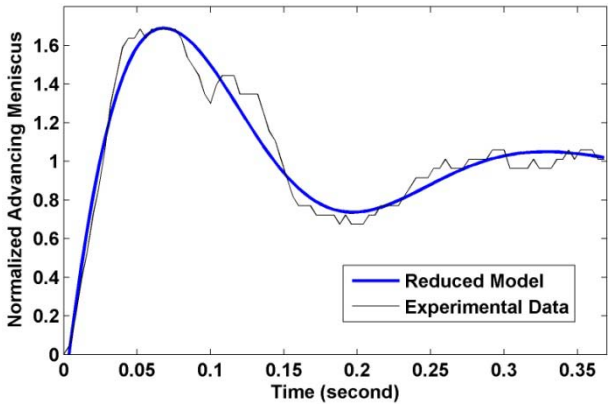

FIGURE 10. MENISCUS TRANSIENT RESPONSE (65mm/s)

TABLE 3. TRANSIENT CHARACTERISTICS (60mm/s)

Reduced Models: $\omega_n = 26.6$ rad/s; $\varsigma = 0.158$ $K_- = 0.0154$; $K_+ = 0.0187$		
	Advancing	**Receding**
Model 1:	$T_- = -0.028$ s	$T_+ = -0.0160$ s
Model 2	$T_- = T_+ = 0$	

TABLE 4. TRANSIENT CHARACTERISTICS (65mm/s)

Advancing meniscus (65mm/s)	
$\varsigma = 0.325$	$K_- = 0.0149$
$\omega_n = 25.9$ rad/s	$T_- = 0$

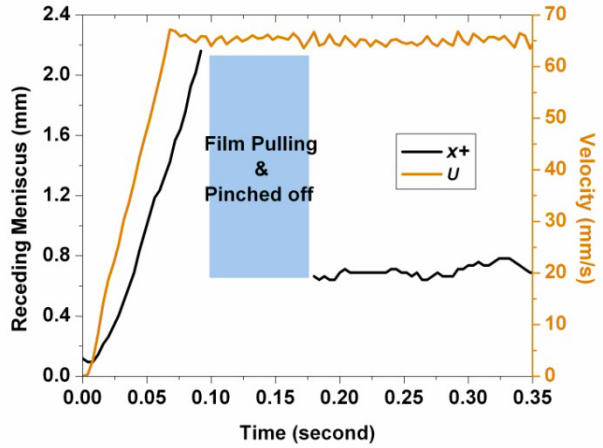

FIGURE11. STAGE VELOCITY AND RECEDING MENISCUS (65mm/s)

The followings are observations drawn from the results:

1) The critical scan speed, beyond which liquid loss occurs at the receding meniscus, has a value between 60mm/s and 65mm/s. The phenomena can be explained as follows: when the viscous force (that increases with the scanning velocity) is greater than the surface tension at the receding meniscus, a liquid tail would be dragged from the immersion fluid (also called film pulling). The dragged film would be pinched off and left into droplets due to surface tension [13], which results in liquid loss.

2) Figures 8(a) and 8(b), where the dynamic contact angles are defined in Fig. 2(b), compare the developing contact angles at two scan speeds; 60mm/s and 65mm/s. The diagonally opposite contact angles (θ_{AU} and θ_{RL}; or θ_{AL} and θ_{RU}) behave similarly; both angles of each pair reach a common steady state value. The pair (θ_{AU} and θ_{RL}) decreases while the other pair increases; both pairs mirror each other about their initial steady state values. When film pulling occurs at the scan speed of 65mm/s as shown in Fig. 8(b), θ_{RL} decreases nearly to zero and then the dragged liquid tail shrinks followed by pinched off under the influence of surface tension.

3) The dynamics of the advancing and receding menisci with a scan speed of 60mm/s are shown in Fig. 9(a) and 9(b) respectively. In each plot, two reduced models (with and without the effect of zero), which characterize the transient response with parametric values derived from experimental data using MATLAB System Identification Toolbox, are given in Table 3. Both the reduced 2nd order models agree qualitatively well with experimental data, and show that $T_{\pm}$ has a very small value and is negative. Since a_r and $b_{\pm}$ are positive,

$$T_{\pm} \approx 0 \;\Rightarrow\; k_c \approx -\left(\frac{1}{a_r}\right)\left(\frac{b_+ b_-}{b_+ + b_-}\right)$$

The negative value for the spring constant k_c can be explained as follows. Since x_+ stretches more than x_-, the liquid for m_c flows toward the *x*-*z* plane due to the continuity of fluid flow and hence the meniscus displacement x_c contracts inwards (in the same direction of the surface tension) instead of restoring outwards as an ideal mechanical spring normally does. The zero has an effect similar to a pure time delay at scan speed of 60mm/s:

$$1 - T_{\pm} s \approx e^{-T_{\pm} s}$$

CONCLUSION

A method has been presented to formulate a lumped parameter model for analyzing the immersion fluid dynamics. This model takes the surface tension forces and viscous frictional forces as spring-damper pairs which expand or retract about the equilibrium state during scanning. In order to obtain a tractable experimental model, the lumped-parameter model is reduced to a 2nd order model, and validated against the actual liquid transient response, which agrees qualitatively well. The findings provide a rational basis for taking an in-depth understanding of the 3-D fluid dynamic behavior. The results also indicate the spring k_c plays a role of a pure time delay in the reduced model and helps to relieve the mass increase towards the *x*-*z* plane, which may result in liquid loss from receding contact line. But this effect will fail with respect to the critical velocity because the buffer liquid in y-direction cannot take a quick response with the delay characteristic. More research work is being conducted to develop control strategies against liquid loss under increasingly high scan speed.

ACKNOWLEDGMENTS

This project has been financially supported by Natural Science Foundation of China (91023015) and National Key Project (2012ZX02701003).

REFERENCES

[1] Chen, W.Y., Chen, Y., Zou, J., Fu, X., Yang, H.Y., Ruan, X.D., and Gong, G.F., 2009. "Effect of liquid dispensing on flow field for immersion lithography", *J. Vac. Sci. Technol. B*, 27(5), pp 2192-2199.

[2] Owa, S., Nagasaka, H., "2003 Immersion lithography exposure tool update", *2003 Immersion lithography workshop*, San Jose, CA.

[3] Mulkens, J., Flagello, D., Streefkerk, B., and Graeupner, P., 2004. "Benefits and limitations of immersion lithography", *J. Microlith., Microfab., Microsyst.*, 3(1), pp 104-114.

[4] EI-Morsi, M., Nellis, G., Schuetter, S., Van Peski, C., Grenville, A., 2005. "Full wafer simulation of immersion fluid heating", *J. Vac. Sci. Technol. B*, 23(6), pp 2596–2600.

[5] Burnett, H., Shedd, T., Nellis, G., El-Morsi, M., Engelstad, R., Garoff, S., and Varanasi, K., 2005. "Control of the receding meniscus in immersion lithography", *J. Vac. Sci. Technol. B*, 23(6), pp 2611-2616.

[6] Schuetter, S., Shedd. T., Doxtator, K., Nellis, G., Van Peski, C., Grenville, A., Lin, S.H., and Owe-Yang, D.C., 2006. "Measurements of the dynamic contact angle for conditions relevant to immersion lithography". *J. Microlith., Microfab., Microsyst.*, 5(2) , 023002.

[7] Schuetter, S., Shedd. T., and Nellis, G., 2007. "Prediction of the velocity at which liquid separates from a moving contact line", *J. Micro/Nanolith. MEMS MOEMS*, 6(2), pp 023003.

[8] Harder, P.M. and Shedd, T.A., 2008. "Improved model for liquid loss at a dynamic contact line including behaviors of high-index fluids", *J., Micro/Nanolith., MEMS MOEMS*, 7(3), 033002.

[9] Winkels, K.G., Peters, I.R., Evangelista, F., Riepen, M., Daerr, A., Limat, L., and Snoeijer, J.H., 2011. "Receding contact lines From sliding drops to immersion lithography", *Eur. Phys. J. Special Topics*, 192, pp195-205.

[10] Kim, H., Grosse, S., Elsinga, G.E., and Westerweel, J., 2011. "Full 3D-3C velocity measurement inside a liquid immersion droplet", *Exp. Fluids*, 51, pp 395-405.

[11] Bush, J.W.M. and Aristoff, J., 2003. "The influence of surface tension on the circular hydraulic jump", *J. Fluid Mech.*, 489, 229-238.

[12] Munson, B.R., and Young D.F., Okiishi, T.H., Huebsch, W.W, 2010. Fundamentals of fluid mechanics, 6th, Wiley, Chap. 6, pp 311-312.

[13] Chen, Y., Lee, K.-M., and Fu X., 2011. "Effect of upper surface characteristics on meniscus stability in immersion flow field", *Microelectron Eng.*, 88, pp. 1939-1943.

[14] Gonzalez, R.C., Woods, R.E., and Eddins, S.L., 2009. Digital image processing using MATLAB, 2nd, Gatesmark Publishing, Chap. 9, pp. 359-366.

[15] Steven, C.C., and Raymond, C., 2010. Numerical methods for engineers, 6th, McGraw Hill, Chap. 17, pp 440-459.